Particle and Energy Transport in the SOL of DIII-D and NSTX

J.A. Boedo 1), R.J. Maqueda 2), D.L. Rudakov 1), G.R. McKee 3), H. Kugel 4), R. Maingi 5), N. Crocker 6), R.A. Moyer 1), V.A. Soukhanovskii 7), J. Menard 4), J.G. Watkins 8), S.J. Zweben 4), D.A. D'Ippolito 9), T.E. Evans 10), M.E. Fenstermacher 7), M. Groth 7), E.M. Hollmann 1), C.J. Lasnier 7), J.R. Myra 9), L.A. Roquemore 4), W.P. West 10), and L. Zeng 6)

1) University of California-San Diego, La Jolla, California, USA
2) Nova Photonics, Princeton, New Jersey, USA
3) University of Wisconsin-Madison, Madison, Wisconsin, USA
4) Princeton University, Princeton, New Jersey, USA
5) Oak Ridge National Laboratory, Oak Ridge, Tennessee, USA
6) University of California-Los Angeles, Los Angeles, California, USA
7) Lawrence Livermore National Laboratory, Livermore, California, USA
8) Sandia National Laboratories, Albuquerque, New Mexico, USA
9) Lodestar Research Corp, Boulder, Colorado, USA
10) General Atomics, P.O. Box 85608, San Diego, California 92186-5608, USA

e-mail contact of main author: boedo@fusion.gat.com

Abstract. The far scrape-off layer (SOL) radial transport and plasma-wall contact is mediated by intermittent and ELM-driven transport. Experiments to characterize the intermittent transport and ELMs have been performed in both DIII-D and NSTX under similar conditions. Both intermittent transport and ELMs are comprised of filaments of hot, dense plasma ($n_e \sim 1\times10^{13}$ cm^{-3}, $T_e \sim 400$ eV) originating at the edge, transport both particles and heat into the SOL by convection, increasing wall interaction and causing sputtering and impurity release. Both intermittent filaments and ELMs leave the pedestal region at speeds of ~0.5-3 km/s, losing heat and particles by parallel transport as they travel through the SOL. The intermittency shows many similarities in NSTX and DIII-D, featuring similar size (2-5 cm), large convective radial velocity, "holes" inside and peaks outside the LCFS which quickly decay and slow down with radius. Whereas in DIII-D the intermittency decays in both intensity and frequency in H-mode, it chiefly decays in frequency in NSTX. In the low collisionality ($\nu^* = \pi R_{q95}/\lambda_C$) ($\nu^*$~0.1, $N_G \sim 0.3$) case, the ELMs impact the walls quite directly and account for ~90% of the wall particle flux, decreasing to ~30% at ($\nu^* \sim 1.0$, $N_G > 0.6$).

INTRODUCTION

Recent results show that the SOL density and temperature profiles in tokamaks and other devices are often non-exponential and flat, suggesting that perpendicular transport in these conditions is much larger than expected. Intermittent, radial ballistic transport, mediated by plasma filaments [1-3] is the vehicle for the enhanced radial transport and has been extensively documented in wide range of devices. Work on characterizing the transport, finding its origins and comparing with numerical simulations has been performed in linear devices [4,5], stellarators [6-9], (Weldenstein [10], Weldenstein VII-AS [11]), tokamaks [12,13], ALCATOR C-Mod [14-17], DIII-D [18-24], JT-60U [25,26], ASDEX [27], ASDEX-Upgrade [28-30], JET [31-34], CASTOR [35], and TCV [36]). Its statistical properties have been examined [37,38] via the probability distribution function (PDF) [39]. The intermittent objects are born in the vicinity of LCFS at the low field side (LFS) of the torus, presumably as a result of interchange instability [40-43], and move towards the wall due to $\mathrm{E}\times\mathrm{B}$ drifts [1,3]. Modeling of the tokamak edge plasmas [44-46] incorporating this transport have shown that under certain conditions plasma contact with the main chamber wall may be significant — even when the distance to the wall is large compared with the density decay

length existing at the separatrix. Additionally, there is an extensive body of work imaging the edge of various devices with fast cameras [2,47,48] and beam emission spectroscopy (BES) [49] which show these objects as moving plasma filaments. ELMs, although of different origin as ballooning/peeling instabilities [50,51], have similar dynamics once in the SOL [34,52] and consist of a collection of bursts that travel radially at speeds of 1-3 km/s and rotate toroidally as they decay. The ELM plasma travels ballistically and strikes the wall with a flux dependant on collisionality/density [52,53], just as the intermittent filaments and an important question is what is the relative particle flux due to these two sources [54].

Plasma interaction with the main chamber wall is of critical importance for next-step fusion devices such as ITER and it should be managed in order to prevent damage to the first wall elements and core plasma contamination with impurities. Comparative studies among devices are invaluable to gain insight on the basic physics of the origin of intermittency and the fundamental parameters driving the radial transport. Since inter-ELM intermittent particle fluxes can exceed ELM-mediated fluxes, understanding the source of intermittent transport and its dependence on plasma parameters is critical for ITER.

RESULTS

Experiments to evaluate the intermittent transport and its variation with density/collisionality were performed in both NSTX (I_p 0.80 MA, B_t=0.45 T, P_{in}=1 MW, q_{95}=7, W=0.2 MJ, V_{pl}=11 m^3) and DIII-D (I_p=1 MA, B_t = 2 T, P_{in} = 1 MW, q_{95} = 4.6, W=0.16 MJ, V_{pl}=18.7 m^3) in both L-mode and H-mode discharges by scanning the line-averaged density. In DIII-D the density can be tightly controlled and the scan was performed in a shot-to-shot basis, as shown in Fig. 1, whereas in NSTX the density was allowed to ramp up naturally and data was taken at different times, as shown in Fig. 2(d). The density was scanned over a wide range, in terms of the Greenwald fraction ($N_G = n_e \pi a^2 / I_p$) from $N_G \sim 0.12$ to $N_G \sim 0.5$ in DIII-D and from $N_G \sim 0.3$ to $N_G \sim 0.8$ in NSTX. The density scan is reflected by changes in the edge SOL profiles in both machines [Figs. 2(a-c) and 3]. These changes are concomitant with modifications in the microscopic behavior of the fluctuations as shown next.

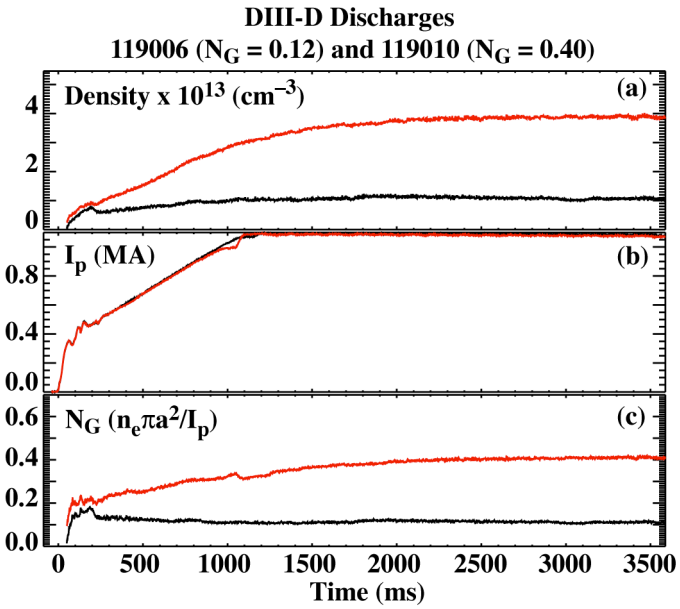

FIG. 1. Time evolution of two otherwise identical DIII-D discharges with different densities.

Pedestal/SOL measurements in DIII-D, shown in Fig. 4, indicate that: (1) the SOL widens and flattens as N_G is increased as seen in the I_{sat} profile [Fig. 4(a)], (2) the fluctuation rms level in I_{sat} [Fig. 4(b)] increases with N_G, (3) the E_θ rms levels [Fig. 4(c)] are mostly unaffected by the scan, and (4) changes are most noticeable at the highest N_G in both devices (NSTX in Fig. 5). The E_θ rms signal can be interpreted as flux $\Gamma = nV_r$, where $V_r^{rms} = E_\theta^{rms} / Bt$ and therefore the transport increase in DIII-D is mostly due to increase in the density of the

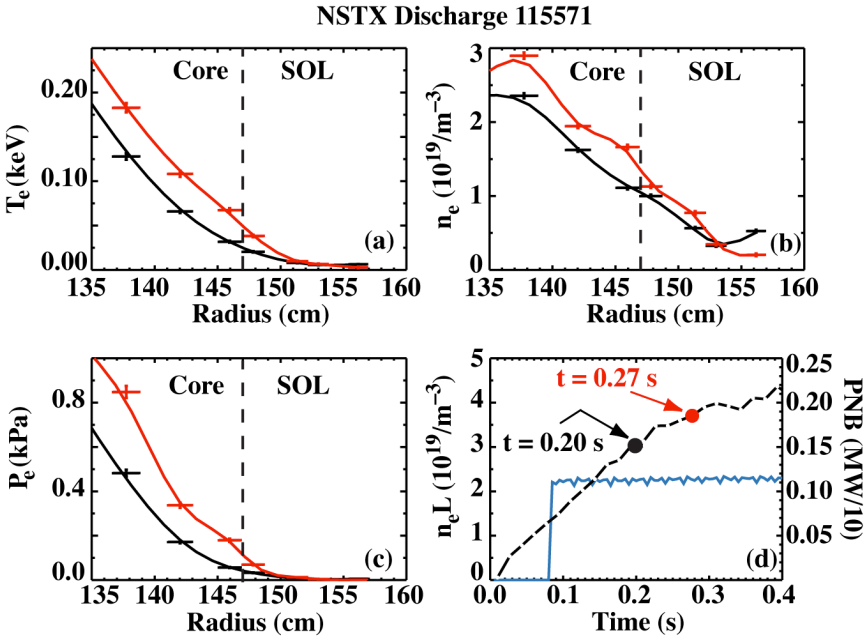

FIG. 2. NSTX Thomson scattering edge/SOL profiles of (a) temperature, (b) density, (c) electron pressure. The time evolution of the density and NBI power are shown in (d).

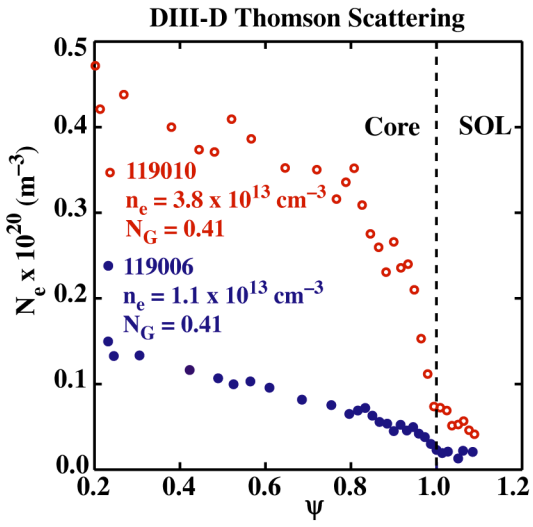

FIG. 3. DIII-D Thomson scattering profiles for the discharges shown in Fig. 1 at 2500 ms and averaged over 200 ms.

intermittent objects. In NSTX however, we observe that: (1) the SOL [Fig. 5(a)] flattens only at the highest densities, (2) the I_{sat} rms levels [Fig. 5(b)] clearly increase with density in the edge/LCFS but little in the SOL, (3) the I_{sat} rms levels decrease with radius, indicating dissipation of the intermittent filaments, and (4) the E_θ rms levels [Fig. 5(c)] are mostly unaffected by the scan. Note that the E_θ rms levels are similar at the LCFS in both devices (~1200 V/m in DIII-D and ~ 900 V/m in NSTX) but due to NSTX having a much lower *Bt* at the LCFS (~ 1.8 T at DIII-D versus ~ 0.25 T at NSTX, a factor of ~7), they correspond to much higher radial velocities at NSTX (~ 1 km/s versus ~ 3.5 km/s) for these low power L-mode conditions than in DIII-D. It is also noticeable that the rms velocity ***decreases*** rapidly with radius.

Numerical simulations and other theoretical works [55-59] have proposed turbulence at the LCFS or thereabouts propagating into the SOL as the origin of the intermittency, in particular, the interchange instability [56] seems to reproduce the measured results well. An element of these models is the presence of density "holes" in the birth region of the intermittency; therefore, the data was tested by calculating the skewness of various signals and statistical analysis indicates that holes/peaks appear as negative/positive skewness [22]. The results are shown in Fig. 6(a,b) for NSTX and Fig. 6(c) for DIII-D. In the data we can observe: (1) the skewness of the I_{sat} signal [Fig. 6(a)] is negative (≃1.2) inside the LCFS, crosses zero and becomes positive in the SOL; (2) there is a clear dependence of the skewness with density in the SOL (near SOL, not in the shadow of structures) that becomes apparent at the highest N_G values (0.54–0.67); (3) similar, although less pronounced, behavior is observed in the E_θ rms [Fig. 6(b)] signal indicating inward radial velocity for some objects within the LCFS. The BES density signal in DIII-D [Fig. 6(c)] show similar behavior, suggesting the presence of a common mechanism in both devices.

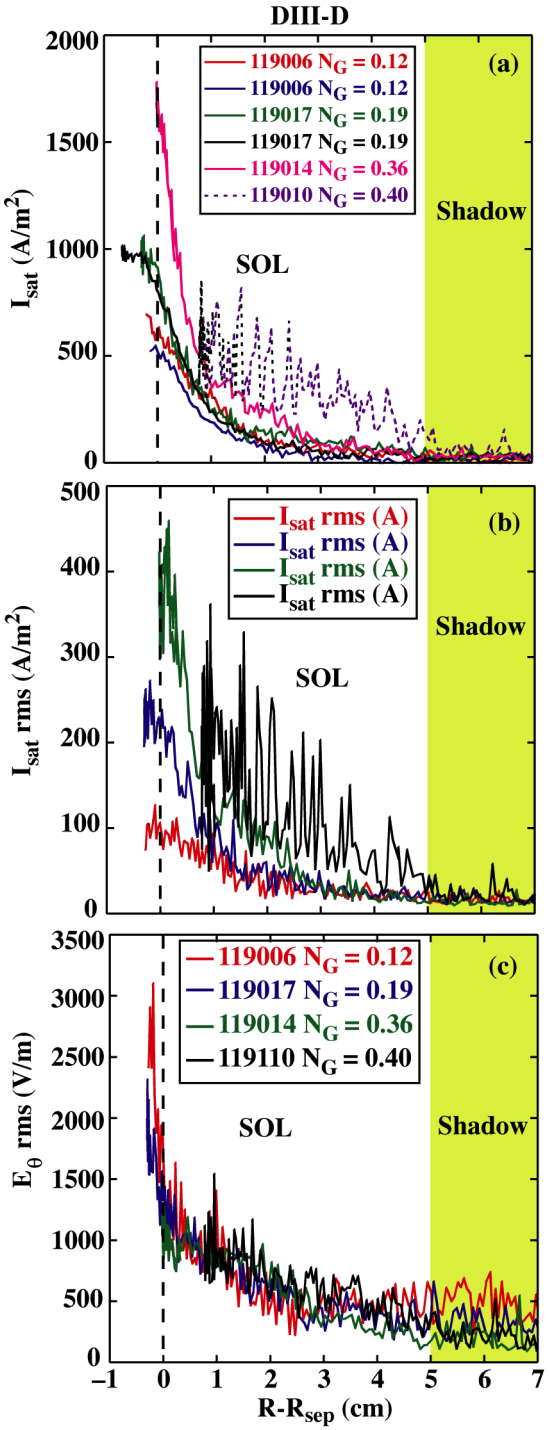

FIG. 4. DIII-D reciprocating probe profiles of (a) I_{sat}, (b) I_{sat} rms and (c) E_θ rms. Dashed line indicates the EFIT separatrix.

Imaging of the intermittent structures permits dynamics visualization and quantitative measurements of velocity, poloidal and radial extent, etc. In NSTX, the intermittency is imaged with high spatial and temporal resolution with the gas puff imaging (GPI) [60]. It is clear that the intermittent objects are born from edge turbulence and that both broadband turbulence and intermittent objects are substantially reduced during H-mode with respect to the Ohmic or L-mode regimes. In Fig. 7(a-c) images from a ~23 x 23 cm radial versus poloidal portion of the edge just above the outer midplane are shown. Turbulence behavior varies widely from a turbulence level just above that measurable, a "quiescent" H-mode [Fig. 7(b)], to that approaching L-mode level shown in Fig. 7(c), at least for brief periods of time. The camera data allows the determination of poloidal and radial correlation lengths (4-9 cm and 2-6 cm respectively), poloidal velocities (up to 5 km/s in the ion diamagnetic drift direction) and radial velocities (up to 2 km/s outwards) [48,61]. The most significant change in the turbulence from L-mode to H-mode is a decrease in the fluctuations in the poloidal velocity of the turbulence, as if the flow was more "frozen" in H-mode. In DIII-D, the intermittent objects can be observed in 2D [Fig. 7(d)] with the BES system [49] which encompasses a smaller (5 x 6 cm) area, with lower resolution but better sensitivity than GPI. The intermittent objects look remarkably similar in both devices in size and dynamics. The measured intermittency radial velocity in the scrape-off layer appears to be bounded by a minimum velocity which can be explained theoretically [62] as imposed by a "sheath-connected" regime and a maximum velocity set by the "resistive-ballooning" regime. Intermittency changes character in H-mode; while in DIII-D the intensity and frequency of the filaments decrease as compared to L-mode, in NSTX only the frequency is reduced.

INTERMITTTENT VS ELM-MEDIATED TRANSPORT

NSTX and DIII-D showcase an abundance of ELM regimes [63] which allow comprehensive studies to be performed. Probe data taken in NSTX during Type I ELMs (Fig. 8), which consist of ~1-2 ms long sequence of ~5-30 fast bursts of hot, dense plasma, look identical to

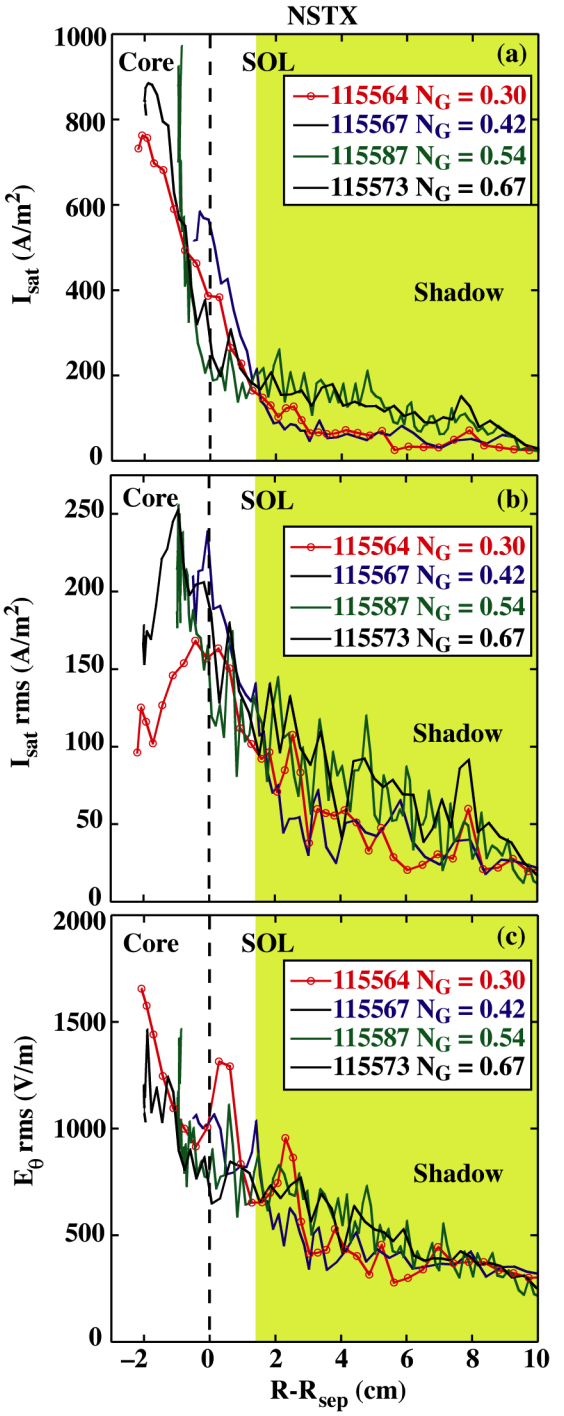

FIG. 5. NSTX reciprocating probe profiles of (a) I_{sat}, (b) I_{sat} rms and (c) E_θ rms. Dashed line indicates the LRDFIT separatrix.

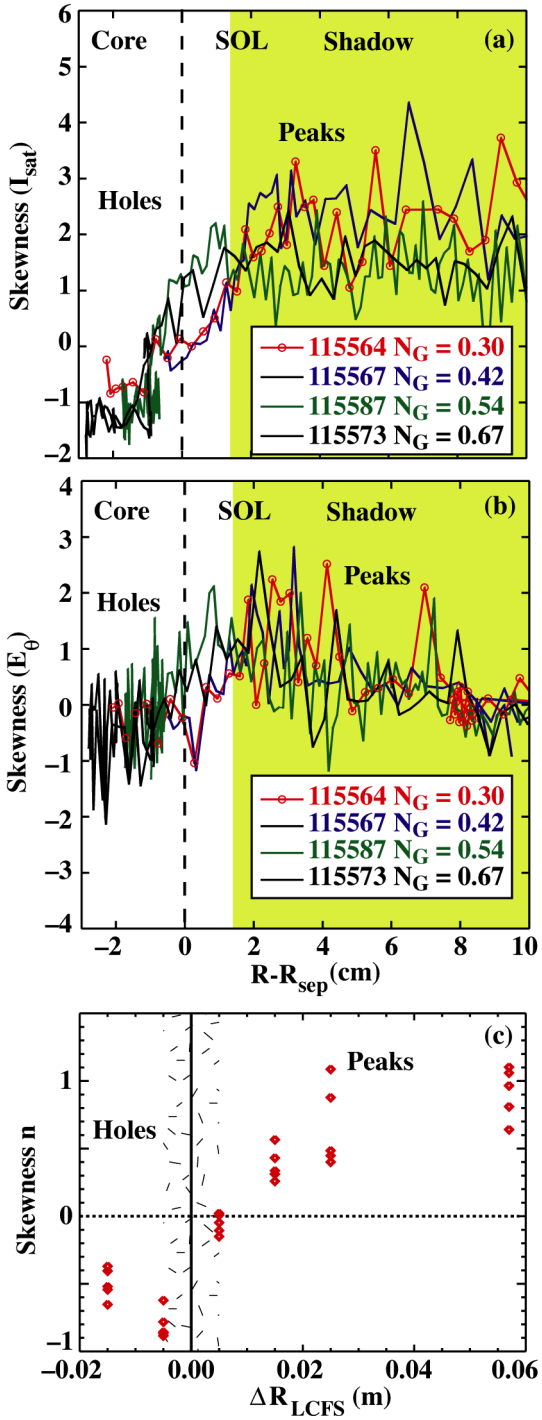

FIG. 6. NSTX reciprocating probe profiles of (a) skewness (I_{sat}), (b) skewness of (E_θ) and (c) skewness of DIII-D BES data showing the transition from holes to bursts at the LCFS in both NSTX and DIII-D. Dashed line indicates the LRDFIT or EFIT separatrix.

data obtained from DIII-D [52]. As the NSTX probe moves, a series of ELM-induced plasma filaments strike it and therefore a plot of the peak saturation current ($\propto n_e\sqrt{T_e}$) versus radius can be assembled. A decay length of 1.7 cm for I_{sat}, shown in Fig. 8(a), is determined by an exponential fit to the data; and the filament's velocity, calculated as $V_r = E_\theta / B_T$, is of the order of 400 m/s at the LCFS [Fig. 8(b)] and features a decay length of ~7 cm; similar numbers as those in DIII-D [52]. In

DIII-D it is found that whereas the energy is quickly reduced in the ELMs at all collisionalities, featuring a short (1-2 cm) decay length [52], the density decay length is highly dependent on collisionality. For low collisionality ($N_G \sim 0.5$, $\nu^* \sim 0.1$), the ELM density decay length is long (~13 cm) indicating that the ELM particle flux impacts the walls quite directly whereas at high collisionality ($N_G \sim 0.8$, $\nu^* \sim 1$), the particle flux decays in a short ~ 3.5 cm. This change is concomitant with the transformation of ELMs into more grassy, lower amplitude types.

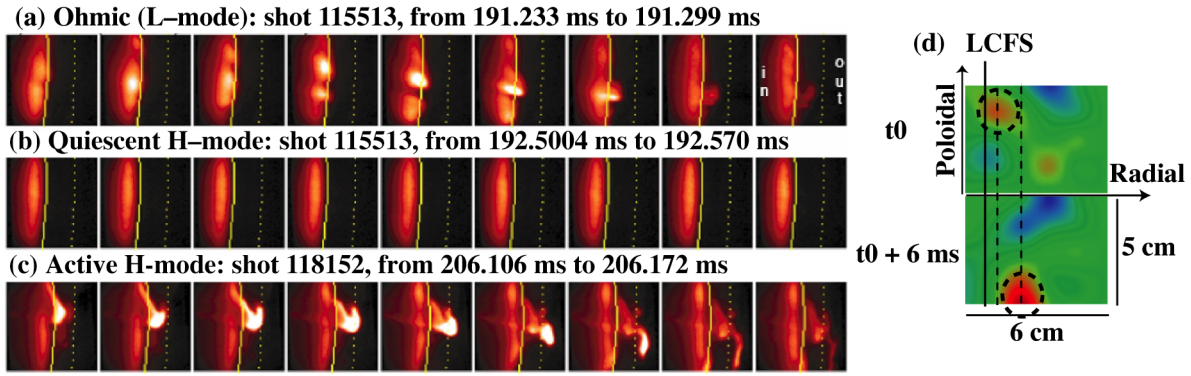

FIG. 7. Imaging data (a-c) from the GPI system at NSTX showing intermittent behavior during Ohmic, quiescent H-mode and active H-mode respectively. Sequence of images obtained at 120,000 frames/s with each image exposed for 3 ms. A deuterium puff is injected from the right and D_a light is imaged. Each image corresponds to ~23 x 23 cm (solid line: separatrix, dotted line: antenna limiter shadow). Two DIII-D BES frames, (d), taken 6 μs apart showing a coherent object leaving the separatrix (solid line) and moving radially and poloidally into the SOL. Frames cover a 5 x 6 cm area.

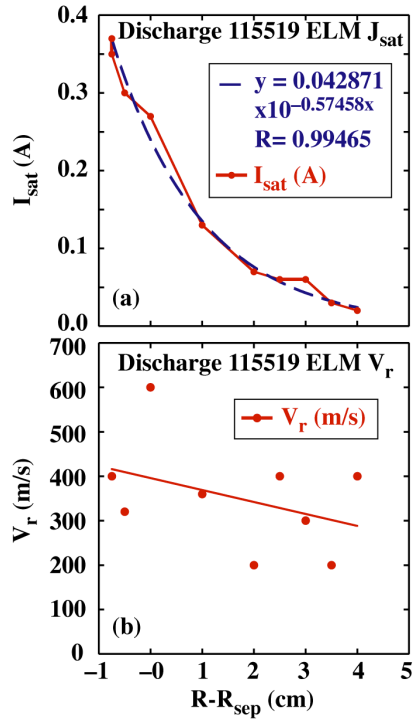

FIG. 8. NSTX reciprocating probe data showing (a) decay of ELM amplitude (I_{sat}) with radius and, (b) ELM radial velocity ($V_r = E_\theta / Bt$) decaying slowly into the SOL.

A weakening of the ELM-induced radial particle flux with collisionality (ELMs become grassier and smaller at high collisionality), coupled with a simultaneous strengthening of the intermittent transport demands a quantification of the relative importance of these two transport vehicles. Figure 9 compares various ELM and inter-ELM SOL parameters (T_e, n_e, $\tilde{n}_e$ and $q_{||}$) in L- and H-mode for similar collisionality ($N_G \sim 0.5$, $\nu^* \sim 0.4$) showing that Type I ELM density, temperature and fluctuations, can be momentarily comparable, and even higher, than L-mode ones in most conditions but is dependent on the ELM duty cycle (and discharge density). Most remarkably, recent DIII-D work using collisionality scans [54], shown in Fig. 10, revealed that the fraction of the ion particle flux to the wall due to ELMs to the total ion flux (defined as $f_{ELM} = \int_{ELM} I_{si}dt / \int_{Total} I_{si}dt$ [54]) account for ~ 90% of the wall particle flux at low collisionality (expressed as the Greenwald fraction N_G) $N_G \sim 0.3$, decreasing to ~30% at $N_G \sim 1.0$.

The implications of the previous data are significant since for high N_G ITER discharges: (1) the

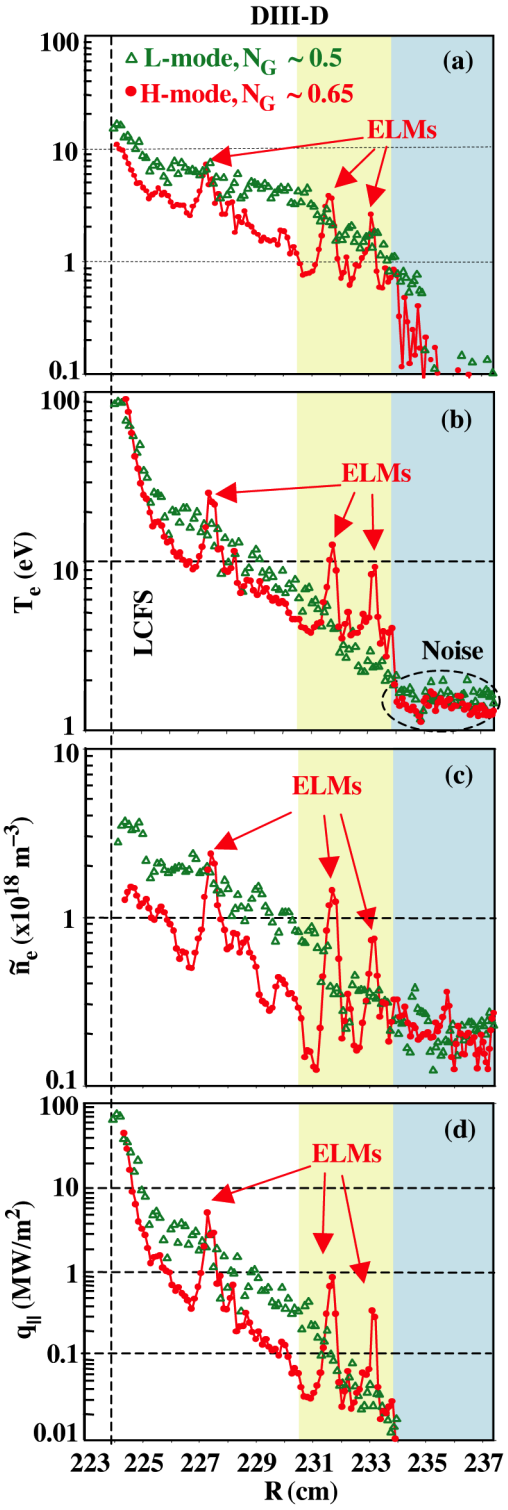

FIG. 9. Radial profile of n_e (a), T_e (b), $\tilde{n}_e$ fluctuations (c) and parallel heat flux (d) for LSN, 1.1 MA, otherwise similar L- and H-mode discharges.

wall- plasma flux increases to at least 50% of the total, and (2) the intermittent particle transport will dominate at the wall. This is both good news and bad news since the load on the divertor is significantly reduced but it requires mitigation techniques at the walls and diagnostics.

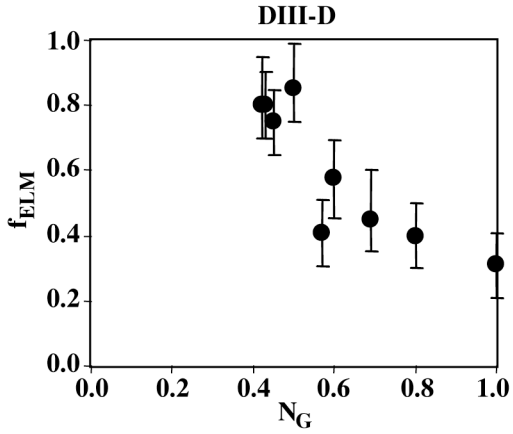

FIG. 10. Ratio of the ELM-mediated ion flux to the total flux at the wall as function of N_G.

Work supported by the U.S. Department of Energy under DE-FC02-04ER54698, DE-FG02-04ER54758, DE-FG03-01ER54615, W-7405-ENG-48, DE-AC05-00OR22725, DE-FG02-89ER53296, DE-AC04-94AL85000, and DE-AC02-76CH03073.

REFERENCES

[1] KRASHENINNIKOV, S.I., Phys. Lett. A **283** (2001) 368.
[2] ZWEBEN, S.J., Phys. Fluids **28** (1985) 974.
[3] D'IPPOLITO, D., et al., Phys. Plasmas **9** (2002) 222.
[4] NIELSEN, A.H., et al., Phys. Plasmas **3** (1996) 1530.
[5] LEHMER, R.D., Ph.D. thesis, Univ. California Los Angeles, UCSDENG-032, (1996).
[6] SANCHEZ, E., et al., Phys. Plasmas **7** (2000) 1408.
[7] LYON, J.F., et al., Fusion Technol. **10** (1986) 179.
[8] GARCIA-CORTES, M.A. et al., Phys. Fluids B **4** (1992) 4007.
[9] GARCIA-CORTES, I., et al., Plasma Phys. Control. Fusion **42** (2000) 389.
[10] JOSEPH, B.K., et al., Phys. Plasmas **4** (1997) 4292.
[11] RENNER, H., et al., Plasma Phys. Control. Fusion **37** (1995) A53.
[12] JHA, R., SAXENA, Y.C., Phys. Plasmas **3** (1996) 2979.
[13] FILIPPAS, A.V., et al., Phys. Plasmas **2** (1995) 839.

[14] UMANSKY, M.V., et al., Phys. Plasmas 5 (1998) 3373.
[15] LaBOMBARD, B., et al., Phys. Plasmas **8** (2001) 2107.
[16] TERRY, J.L., et al., Phys. Plasmas **10** (2003) 1739.
[17] ZWEBEN, S.J., et al., Phys. Plasmas **9** (2002) 1981.
[18] WATKINS, J.G., et al., J. Nucl. Mater. **196–198** (1992) 829.
[19] WADE, M., et al., J. Nucl. Mater. **266–269** (1999) 44.
[20] BOEDO, J.A., et al., Phys. Plasmas 8 (2001) 4826.
[21] RUDAKOV, D.L., et al., Plasma Phys. Control. Fusion 44 (2002) 717.
[22] BOEDO, J.A., et al., J. Nucl. Mater. 313–316 (2003) 813.
[23] BOEDO, J.A., et al., Phys. Plasmas **10** (2003) 1670.
[24] FENSTERMACHER, M.E., et al., Plasma Phys. Control. Fusion **45** (2003) 1597.
[25] ASAKURA, N., et al., J. Nucl. Mater. **241–243** (1997) 559.
[26] ASAKURA, N., et al., J. Nucl. Mater. **337–339** (2005) 712.
[27] ENDLER, M., et al., Nucl. Fusion **35** (1995) 1307.
[28] NEUHAUSER, J., et al., Plasma Phys. Control. Fusion **44** (2002) 855.
[29] KALLENBACH, A., et al., Nucl. Fusion **43** (2003) 573.
[30] HERRMANN, A., et al., Plasma Phys. Control. Fusion **46** (2004) 971.
[31] GHENDRIH, Ph., et al., J. Nucl. Mater. **313–316** (2003) 914.
[32] GONCALVES, B., et al., Plasma Phys. Control. Fusion **45** (2003).
[33] FUNDAMENSKI, W., et al., Plasma Phys. Control. Fusion **46** (2004) 233.
[34] ENDLER, M., et al., Plasma Phys. Control. Fusion **47** (2005) 219-240.
[35] SOTECKEL, J., et al., Phys. Plasmas **6** (1999) 846.
[36] HORACEK, J., J. Physics (Czechoslovak) **55**(3) (2005) 271-83.
[37] CARRERAS, B., et al., Phys. Plasmas **7** (2000) 3278.
[38] CARRERAS, B.A., Phys. Plasmas **8** (2001) 3702.
[39] SANCHEZ, E., et al., Phys. Plasmas **7** (2000) 1408.
[40] ENDLER, M., et al., Nucl. Fusion **35** (1995) 1307.
[41] NEDOSPASOV, A.V., Sov. J. Plasma Phys. **15** (1989) 659.
[42] GARBET, X., et al., Nucl. Fusion **31** (1991) 967.
[43] SARAZIN, Y., Phys. Plasmas **5** (1998) 4214.
[44] UMANSKY, M.V., et al., Phys. Plasmas **5** (1998) 3373.
[45] PIGAROV, A.Yu., et al., Phys. Plasmas **9** (2002) 1287.
[46] PIGAROV, A.Yu., et al., J. Nucl. Mater. **313–316** (2003) 1076.
[47] MAQUEDA, R.J., et al., Rev. Sci. Instrum. **74** (2003) 2020.
[48] ZWEBEN, S.J., et al., Nucl. Fusion **44** (2004) 134.
[49] McKEE, G.R., et al., Rev. Sci. Instrum. **70** (1999) 913.
[50] CONNOR, J.W., et al., Phys. Plasmas **5** (2002) 2687.
[51] SNYDER, P.B., et al., Phys. Plasmas **9** (2002) 2037.
[52] Boedo, J.A., Phys. Plasmas **12** (2005) 072516.
[53] LEONARD, A.W., et al., to be published in J. Nucl. Mat. (2006).
[54] RUDAKOV, D.L., et al., Nucl. Fusion **45** (2005) 1589-1599.
[55] BIAN, N., et al., Phys. Plasmas **10**(3) (2003) 671-676.
[56] SARAZIN, Y., et al., J. Nucl. Mat. **313-316** (2003) 796-803.
[57] XU, X.Q., Phys. Plasmas **10** (2003) 1773.
[58] RUSSELL, D., et al., Phys. Rev. Lett. **93** (2004) 265001.
[59] MYRA, J., et al., Phys. Plasmas **12** (2005) 092511.
[60] MAQUEDA, R.J., et al., Rev. Sci. Instrum. **74** (2003) 2020.
[61] ZWEBEN, S.J., et al., Phys. Plasmas **13**, 056114 (2006).
[62] MYRA, J.R., et al., this conference.
[63] MAINGI, R., et al. Nucl. Fusion **45** (2005) 1066.